

Online 6DoF Pose Estimation in Forests using Cross-View Factor Graph Optimisation and Deep Learned Re-localisation

Lucas Carvalho de Lima^{1,2}, Ethan Griffiths^{1,3}, Maryam Haghghat³, Simon Denman³,
Clinton Fookes³, Paulo Borges^{1,2}, Michael Brünig² and Milad Ramezani^{1*}

Abstract—This paper presents a novel approach for robust global localisation and 6DoF pose estimation of ground robots in forest environments by leveraging cross-view factor graph optimisation and deep-learned re-localisation. The proposed method addresses the challenges of aligning aerial and ground data for pose estimation, which is crucial for accurate point-to-point navigation in GPS-denied environments. By integrating information from both perspectives into a factor graph framework, our approach effectively estimates the robot’s global position and orientation. We validate the performance of our method through extensive experiments in diverse forest scenarios, demonstrating its superiority over existing baselines in terms of accuracy and robustness in these challenging environments. Experimental results show that our proposed localisation system can achieve drift-free localisation with bounded positioning errors, ensuring reliable and safe robot navigation under canopies.

I. INTRODUCTION

Reliable geo-localisation in forest environments is crucial for executing various robotics tasks ranging from forest inventory and monitoring to search and rescue missions. Traditional localisation methods typically utilise onboard measurements from Inertial Measurement Unit (IMU) [1], [2], lidar [3], or vision [4] to estimate the robot motion over time, further depending on periodic observations from Global Positioning System (GPS) to update pose estimates. However, these methods often struggle in forested areas where GPS signals are frequently lost or degraded under dense canopies, leading to drift and poor localisation.

Alternative solutions based on Simultaneous Localisation and Mapping (SLAM) have been proposed for localisation with drift correction in forested environments [5]. Lidar-based SLAM systems are widely used in forest inventory applications [6]–[8], where they match consecutive scans and extracted landmarks (e.g., trees) using robust data association methods to estimate the robot’s relative motion and correct drift when loop closures are detected. However, in long-range point-to-point navigation tasks—the primary focus of our approach—SLAM methods are inherently prone to drift over long runs in open-loop routes. Even when integrated with GPS, SLAM can provide geo-referenced localisation [3], [9], [10], but the resulting position estimates remain subject to GPS inaccuracies as seen in Figure 1 (bottom).

¹ CSIRO Robotics, DATA61, CSIRO, Brisbane, Australia. E-mails: `firstname.lastname@data61.csiro.au`

² School of Information Technology and Electrical Engineering, The University of Queensland (UQ), Brisbane, Australia.

³ School of Electrical Engineering and Robotics, Queensland University of Technology (QUT), Brisbane, Australia.

*Corresponding author

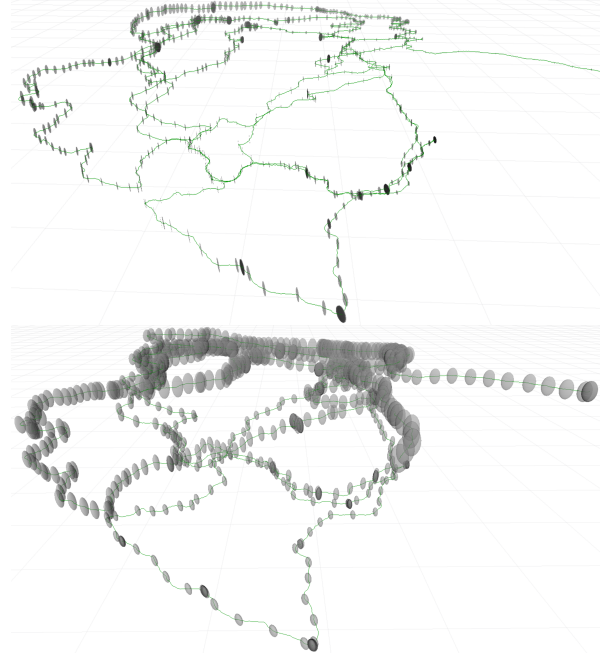


Fig. 1: Uncertainty ellipsoids (1σ) for the proposed factor-graph solutions using the aerial map as an external reference (top) compared to GPS as an external reference (bottom). Ellipsoid scale increased 10x for better visualisation. Grid cell size is 10m.

The primary challenge we address is achieving reliable geo-localisation (Figure 1 (top)) for ground robots in dense forest environments, enabling them to reach target locations over long-range, open-loop trajectories. Inspired by our previous work [11], which also associates aerial and ground data, we introduce a new paradigm for aerial-ground collaboration, offering significant advancements in accuracy and robustness. Our new approach leverages deep-learned re-localisation to position ground robots within the aerial map accurately. Upon the success of re-localisation, we register ground submaps with their aerial correspondences to reliably estimate 6DoF robot poses using factor-graph optimisation and uncertainties derived from data association. This differs from our earlier solution, which relied on Monte Carlo Localisation (MCL) to estimate 3DoF robot poses a-posteriori.

The main contributions are summarised as follows:

- We present an effective online 6DoF geo-localisation system, *FGLoc6D*, for ground robots operating in GPS-degraded environments.
- We formulate ground-to-aerial correspondences as unary factors within factor-graph optimisation inte-

grated with deep-learned re-localisation.

- We validate the proposed pipeline through real-time experiments in challenging environments, demonstrating its robustness and effectiveness.

II. RELATED WORK

We review current localisation pipelines using aerial data and then discuss re-localisation research.

A. Localisation Using Airborne Data

Previous authors have addressed the challenges of ground-to-aerial robot localisation by aligning local range data with maps of building structures and edges derived from satellite imagery [12], [13]. More recent works [14], [15] have introduced models based on transformers [16] to match orthogonal aerial and ground views. Despite impressive results, these methods are not well-suited for environments with complex geometries, such as forests.

Tackling ground robot localisation in natural environments, Vandapel *et al.* [17] match terrain surface meshes with aerial lidar data using spin-image signatures [18]; however, their approach struggles in featureless terrains. Viswanathan *et al.* [19] convert side-view images from onboard cameras into bird’s-eye views to match with satellite imagery using traditional visual features. Shalev and Degani [20] localise a ground robot in orchards by matching canopy edges from low-altitude drone images with a high-altitude image using MCL. Their vision-based method falters in dense forests due to unclear borders between crowns. Hussein *et al.* [21] use Iterative Closest Point (ICP) [22] to align 3D ground lidar data of tree trunks with overhead crown maps; however, their approach is sensitive to errors in crown edge delineation, leading to potential localisation inaccuracies.

Carvalho de Lima *et al.* [11] localise ground robots within an aerial map by extracting cross-view invariant features from trees and using a particle filter to score and match hypotheses. However, their approach estimates only 3DoF poses, making it less effective for uneven terrains. A tightly coupled lidar-inertial localisation on prior ground-view maps using factor graphs is presented in [23]. Although similar to our approach, it is limited to urban areas and 2D occupancy submaps for re-localisation, hence unsuitable for forest areas. Additionally, our method leverages map factors from aerial data for 6DoF pose estimation and a deep-learned re-localisation module tested in complex forest scenarios.

B. Lidar-based Re-localisation

Re-localisation with lidar determines a robot’s pose by matching current scans to a 3D prior map, comprising lidar Place Recognition (PR) and relative transformation calculation. Conventional lidar PR methods, *e.g.*, [24]–[26], encode point clouds into global or local descriptors; however, they struggle in unstructured environments.

Deep-learned approaches, on the other hand, use neural networks to extract features, which are either used directly [27], [28] or aggregated into global descriptors [29], [30] for lidar PR. Combined with a robust estimator such

as RANSAC to remove outliers, local features are used to estimate the relative pose between two point clouds upon success in lidar PR. Methods like EgoNN [31] and LCDNet [32] estimate a relative transformation, with the latter using Optimal Transport (OT) to find correspondences rather than a robust estimator. Similarly, SpectralGV [33] estimates the robot’s localisation and improves PR performance by re-ranking the top-k candidates. A recent pipeline [34] enhances multi-robot localisation with a deep-learned cross-modal module, an auxiliary network in conjunction with deep-learned re-localisation, for greater robustness.

III. METHOD

A. System Overview

We aim to localise a ground robot against a prior aerial lidar map \mathcal{M} that we split into N_A submaps $\{\mathcal{P}_A^{[i]} \in \mathbb{R}^3\}_{i=1}^{N_A}$, each of which covers the same area as the ground lidar point clouds $\{\mathcal{P}_G^{[j]} \in \mathbb{R}^3\}_{j=1}^{N_G}$, where N_G indicates number of ground submaps generated over time.

We formulate the problem as a bipartite graph, $\mathcal{G} = (\mathcal{U}, \mathcal{V}, \mathcal{E})$, consisting of variable nodes \mathcal{V} , in our case robot poses, and factor nodes \mathcal{U} , representing the conditional probability between connected variable nodes. Edges \mathcal{E} in the graph connect factor nodes to variable nodes, signifying the dependency of the factors on the variables.

In our factor graph, we define two types of factors: binary and unary. Binary factors are the odometry factors computed from a lidar-inertial odometry system (Section III-C.1). Unary factors are point cloud registrations between ground and aerial submaps (Section III-C.2).

To solve global localisation, upon generation of a new sub-map, *i.e.*, a query point cloud $\mathcal{P}_G^{[q]}$, we run a deep lidar PR network, described in Section III-B. This compares $\mathcal{P}_G^{[q]}$ with all the submaps $\mathcal{P}_A^{[i]}$ of the prior map to find the top candidate, $\mathcal{P}_A^{[t]}$, using a similarity metric. Initial relative pose $\mathbf{T}'_{MG} \in SE(3)$ between submaps $\mathcal{P}_G^{[q]}$ and $\mathcal{P}_A^{[t]}$ is further estimated using corresponding keypoints (Section III-B). To increase robustness, we apply a fast maximum clique method [35] to find inlier correspondences. We first constrain the matching process to estimate translation $\mathbf{t}' \in \mathbb{R}^3$ and heading angle θ' , assuming that submaps are gravity aligned. This reduces failure in registration in forest areas where well-distributed keypoints are not guaranteed. The full 6DoF registration is later computed using ICP [22]. For verification, we compute a fitness score out of ICP registration to decide the success of re-localisation.

The factor derived from our deep-learned re-localisation module, in conjunction with other factors, is used in factor-graph optimisation to estimate 6DoF robot poses with respect to the aerial map. Figure 2 depicts our proposed pipeline.

B. Ground-Aerial Deep Re-localisation

To localise the robot against the prior map \mathcal{M} , our re-localisation module builds on EgoNN [31], employing a light 3D CNN network to train a global descriptor $d_G \in \mathbb{R}^{256}$ and multiple local embeddings $\{d_{\mathcal{L}_t}\}_{t=1}^M \in \mathbb{R}^{128}$, where t

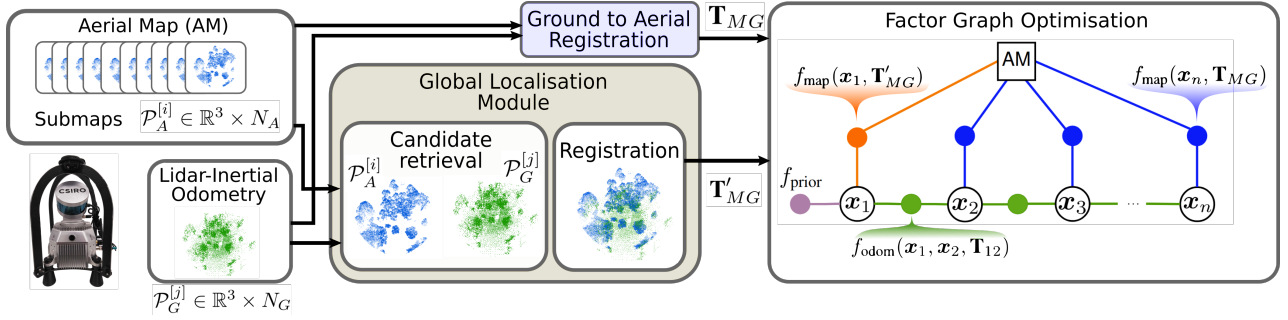


Fig. 2: Block diagram of our proposed pipeline. *FGLoc6D* is composed of a deep-learned module to re-localise the ground robot against an aerial map. It estimates 6DoF robot poses using a fixed-lag smoothing factor graph structure. The factor graph is populated with a prior factor, odometry factors obtained from lidar-inertial odometry, and unary factors representing ground and aerial submap local registrations.

indexes the keypoints detected by USIP [36], in each submap. The global descriptor is derived from pooling feature maps $\mathcal{F}_G \in \mathbb{R}^{K \times 128}$ using GeM [29], with K representing the number of local features. Keypoint descriptors are computed in the local head by processing the local feature map $\mathcal{F}_L \in \mathbb{R}^{M \times 64}$, with local embeddings generated through a two-layer Multi-Layer Perceptron (MLP) followed by a tanh function. Global descriptors are used for place recognition, while local descriptors support metric localisation.

C. Ground-Aerial Factor-Graph Formulation

In our global localisation problem, we seek to estimate the history of robot poses $\mathcal{X} = \{\mathbf{x}_k\}_{k=1}^n$ with respect to an aerial reference map \mathcal{M} , using lidar and IMU measurements.

We formulate the state estimation problem as a factor graph optimisation, where the estimated state vectors are defined as $\mathbf{x}_k = [\mathbf{R}_k, \mathbf{t}_k] \in SE(3)$, with $\mathbf{R}_k \in SO(3)$ representing the orientation and $\mathbf{t}_k \in \mathbb{R}^3$ representing the translation of the ground agent in frame \mathcal{M} . Given the relative transformations between consecutive ground submaps, as well as between ground and aerial, we employ a maximum a posteriori (MAP) approach over the entire set of factors for robot pose estimation:

$$\mathcal{X}^{MAP} = \underset{\mathcal{X}}{\operatorname{argmax}} \prod_{k=1}^n \phi_{\text{map}}(\mathbf{x}_k) \prod_{k=1}^{n-1} \phi_{\text{odom}}(\mathbf{x}_k, \mathbf{x}_{k+1}) \quad (1)$$

where ϕ_{map} and ϕ_{odom} refer to map and odometry factors, respectively.

Assuming the computed transformations are served as conditionally independent measurements corrupted only by white Gaussian noise, Equation (1) can be formulated as the following minimisation problem:

$$\underset{\mathcal{X}}{\operatorname{argmin}} f_{\text{prior}} + \sum_{k=1}^n f_{\text{map}}(\mathbf{x}_k) + \sum_{k=1}^{n-1} f_{\text{odom}}(\mathbf{x}_k, \mathbf{x}_{k+1}) \quad (2)$$

where f_{prior} is the cost function respective to the prior factor. Cost functions f_{odom} and f_{map} are terms respective to the factors associated with the relative transformation between consecutive submaps and transformations between ground and aerial submaps, respectively, weighted by the inverse of their corresponding covariance matrix. These factors are described in the following.

1) Odometry Factors

We employ lidar-inertial odometry, here Wildcat odometry [37], to compute odometry factors between consecutive poses \mathbf{x}_k and \mathbf{x}_{k+1} . These binary factors represent the non-linear least squares linearised locally at the linearisation points \mathbf{x}_k^0 and \mathbf{x}_{k+1}^0 :

$$f_{\text{odom}}(\mathbf{x}_k, \mathbf{x}_{k+1}) = \left\| g(\mathbf{x}_k^0, \mathbf{x}_{k+1}^0) + \mathbf{F}_k \delta \mathbf{x}_k + \mathbf{G}_{k+1} \delta \mathbf{x}_{k+1} - \mathbf{T}_{k,k+1} \right\|_{\Sigma}^2 \quad (3)$$

where g is the mathematical function for odometry and \mathbf{F} and \mathbf{G} are Jacobian matrices with respect to the relative transformation $\mathbf{T}_{k,k+1}$ between consecutive steps k and $k+1$. Vector $\delta \mathbf{x} \triangleq \mathbf{x} - \mathbf{x}^0$ denotes the state update. The notation $\|\cdot\|_{\Sigma}^2$ represents a weighted squared norm, where Σ is the covariance matrix associated with the odometry factors.

2) Map Factors

In our factor-graph optimisation, we obtain ground-to-aerial unary factors utilising Generalised ICP (GICP) [38]. Unlike common ICP, which registers point clouds by minimising the distance point-to-point or point-to-plane, GICP minimises the distance between m local points distributions in a pair of submaps \mathcal{P}_G and \mathcal{P}_A as such:

$$\underset{\mathbf{T}_{MG}}{\operatorname{argmin}} \sum_{i=1}^m \mathbf{d}_i^T (\Sigma_{A_i} + \mathbf{T}_{MG} \Sigma_{G_i} \mathbf{T}_{MG}^T)^{-1} \mathbf{d}_i \quad (4)$$

where, \mathbf{d}_i denotes the distance from the local distribution point i in submap \mathcal{P}_A to the nearest one in submap \mathcal{P}_G after transforming to the map frame by applying \mathbf{T}_{MG} . Matrices Σ_{A_i} and Σ_{G_i} represent the covariance of local distributions in the aerial and ground submaps, respectively.

Considering that the aerial map is the reference and ground-to-aerial submap registrations anchor robot poses to the map, the Hessian matrix relative to the robot pose \mathbf{x}_k can be approximated as:

$$\mathbf{H} \approx \sum_{i=1}^m \left(\frac{\partial \mathbf{d}_i}{\partial \mathbf{x}_k} \right)^T \Omega_i \left(\frac{\partial \mathbf{d}_i}{\partial \mathbf{x}_k} \right) \quad (5)$$

where, $\Omega_i = (\Sigma_{A_i} + \mathbf{T}_{MG} \Sigma_{G_i} \mathbf{T}_{MG}^T)^{-1}$ and $\frac{\partial \mathbf{d}_i}{\partial \mathbf{x}_k}$ is the partial derivative of local distribution distance \mathbf{d}_i evaluated at \mathbf{T}_{MG} . Given that the problem is Gaussian, we serve the inverse of the Hessian matrix as the transformation covariance Λ used in the map factor.

Upon convergence of ground-to-aerial registration, the estimated relative transformation \mathbf{T}_{MG} along with its covariance $\mathbf{\Lambda}$ are used in the map factor as follows:

$$f_{\text{map}}(\mathbf{x}_k) = \|h(\mathbf{x}_k) + \mathbf{J}_k \delta \mathbf{x}_k - \mathbf{T}_{MG}\|_{\mathbf{\Lambda}}^2 \quad (6)$$

where h and \mathbf{J} are the function and the Jacobian matrix respective to transformation \mathbf{T}_{MG} .

Each time a new submap is added, the factor graph undergoes incremental optimisation using iSAM2 [39], which efficiently updates the solution without reprocessing the entire graph.

IV. EXPERIMENTS

We conducted two experiments in separate forest areas at the Queensland Centre for Advanced Technologies (QCAT) in Brisbane, Australia, to evaluate our localisation approach. Ground-based lidar data was gathered using an all-electric four-wheel robotic vehicle and a handheld device [11]. A DJI M300 quadcopter equipped with a GPS antenna for georeferencing purposes and a lidar system captured aerial data for the test areas.

The robot and handheld device were equipped with a perception pack (Shown in Figure 2), featuring a Velodyne VLP-16 lidar sensor mounted on a servo motor inclined at 45° . The sensor, rotating around the vertical axis at 0.5 Hz, provided a 120° vertical field of view, enabling effective scanning of tree crowns. With a 100 m range and a data recording rate of 20 Hz, the lidar system captured detailed environmental information. Additionally, both platforms collected IMU data, with the robotic vehicle also recording wheel encoder measurements.

To establish ground truth for evaluation, we designed the traversals to include loops, which allowed us to leverage an accurate SLAM system with loop-closure detection to mitigate drift and achieve precise pose estimates. We used our lidar SLAM system, Wildcat [37], configured in offline mode with loop closures enabled. This setup allowed the accurate integration of lidar and IMU measurements across the trajectory, resulting in highly precise trajectory estimates.

Our method is implemented in C++ using the Robot Operating System (ROS). Point cloud registration with uncertainty computation was handled using the GICP package implemented in [40], while GTSAM [39] was used for factor-graph optimisation. The algorithm was executed on a unit with an i7-10875H CPU (2.30GHz) with Ubuntu 20.04 as the operating system, and a single NVIDIA Quadro RTX 5000 GPU for re-localisation.

A. Datasets

The following summarises the experiments conducted to evaluate the performance of our approach in diverse forests.

The first experiment (*Forest I*) focused on testing our localisation method in a forest area suitable for ground vehicle traversal. This environment had sparse, mature trees with wide trunks and minimal undergrowth. Lidar data were gathered using a 4-wheel robotic utility vehicle over a 300-meter trajectory.

The second experiment (*Forest II*) aimed to assess the robustness of our method in more complex, long-range scenarios. This forest environment presented challenging terrain with dense vegetation, fallen logs, tall undergrowth, and trees of various sizes, making it non-traversable for robotic platforms. In this case, data was collected using a handheld lidar device, which also recorded IMU and GPS measurements. The experiment covered a 2-kilometre distance over 1 hour and 15 minutes, following loopy paths to create an accurate reference trajectory for evaluation.

Of the *Forest II* experiment, we generated submaps to train our deep re-localisation network. For ground data, we sampled submaps every 5 seconds along the sensor trajectory and cropped them to a horizontal radius of 30 metres centred on the position of the sensor. For aerial data, we used a grid-based sampling approach to generate overlapping submaps with equal coverage to ground submaps. Hence, submaps were sampled every 5 metres along a 2D grid covering the entire aerial map, and all points within a 30-metre horizontal radius were kept. All submaps were then gravity-aligned. To save computation, we downsampled all submaps using a 0.2-metre voxel grid filter.

This produced approximately 1600 ground submaps and 3000 aerial submaps for training the network. We consider ground submaps as queries and all aerial submaps as a database, and reserved a test set of 380 ground queries for evaluation, chosen by randomly selecting two small regions from the ground trajectory.

B. Global Localisation Using Deep Learning

We evaluate the performance of the deep re-localisation module following the submap generation procedure described earlier. We follow the training protocol introduced in [31], using a batch-hard triplet margin loss and Adam [41] optimiser, trained with a learning rate (LR) of $1e^{-3}$ for 160 epochs, reducing the LR by a factor of 10 after epoch 80. To reduce overfitting, we adopt data augmentations including random flips, random rotations of $\pm 180^\circ$, random translation, random jitter, and random block removal. We also pre-process submaps during training by removing uninformative ground points with a cloth simulation filter [42], and perform height offset removal such that the lowest point in each submap begins at $z = 0$. We construct training tuples such that only ground queries and aerial candidates are considered, to better condition the network on our downstream task. Re-localisation is considered successful if at least one of the top- N candidates is within a d metre threshold from the query global position. We report the *AverageRecall@N* (AR@N) metric for a threshold of $d = 5$ m. For metric localisation, we consider registration successful if rotation and translation error are less than 5° and 2 m, respectively.

The deep re-localisation module achieves an AR@1 of 82.4% and AR@5 of 98.4% on the test subset, which we deem sufficient for coarse re-localisation. Of these successful re-localisation requests, we report a metric localisation success rate of 63.8%, with average rotation and translation errors of 2.58° and 0.67 m, respectively. We also report re-

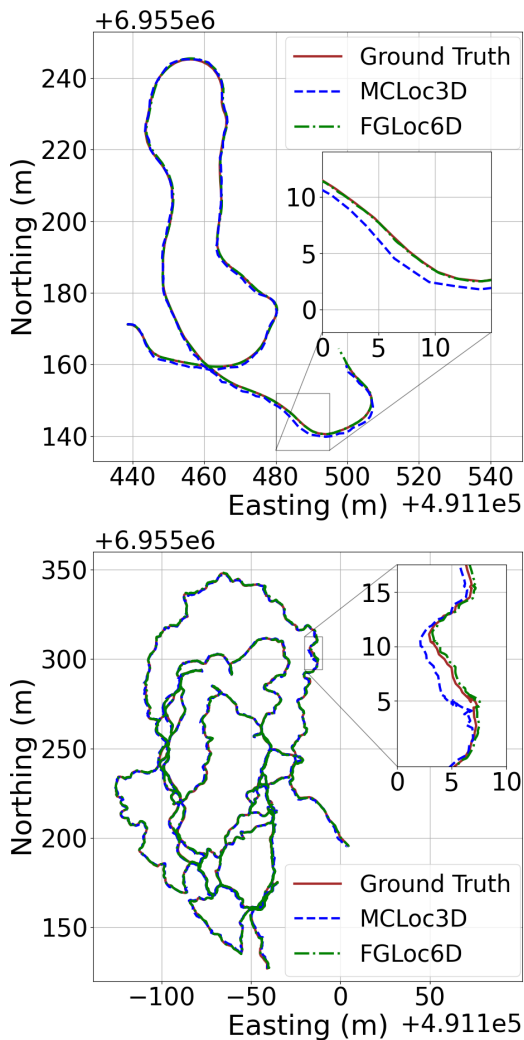


Fig. 3: Trajectory comparison between our proposed localisation method *FGLoc6D*, ground truth (offline Wildcat SLAM [37] with loop-closures) and our previous approach *MCLoc3D* [11] in *Forest I* (top) and *II* (bottom).

sults after further ICP refinement of the estimated transform, resulting in a success rate of 64.4%, and average rotation and translation errors of 2.58° and 0.58 m , respectively.

C. Accuracy Evaluation and Comparison to Baselines

We compared the performance of our proposed global localisation method (*FGLoc6D*) with our previous localisation approach [11], which uses canopy map matching and 3DoF Monte Carlo localisation, referred to as (*MCLoc3D*) in this paper. Additionally, we evaluated baseline methods such as Wheel Odometry (*Wheel Odom*), and two lidar-inertial odometry systems: Wildcat Odometry (*Wildcat Odom*) [37] and LIO-SAM [9]. Wheel Odometry refers to the motion estimation derived from wheel encoders integrated into the four-wheel vehicle. Wildcat Odometry (*Wildcat Odom*) registers features from scans in a sliding window manner, while LIO-SAM performs scan-to-map registration. We disabled loop closure detection in LIO-SAM for a fair comparison, as the goal is to address long-range localisation in open-loop

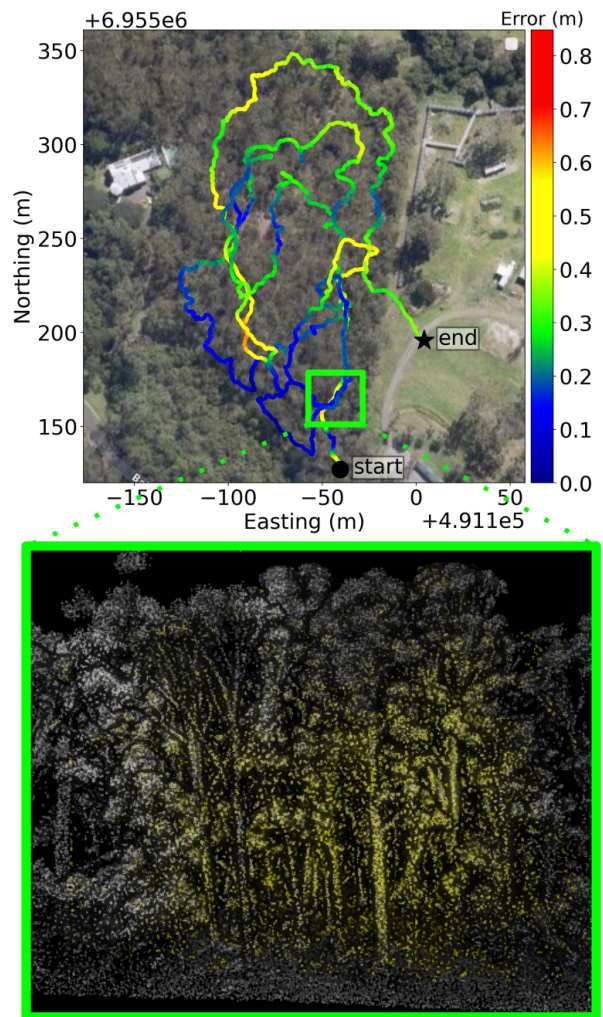


Fig. 4: **Top:** *FGLoc6D* trajectory estimate in *Forest II*. Colour code illustrates absolute translation error compared to ground truth. **Bottom:** A snapshot of ground-to-aerial registration within the area indicated by a square.

scenarios where revisits are not feasible.

Figure 3 compares the trajectories generated by our proposed *FGLoc6D* method and the baseline *MCLoc3D* [11] against the ground truth for the *Forest I* and *II* datasets. In both cases, *FGLoc6D* closely follows the ground truth with minimal positional errors, while *MCLoc3D* exhibits larger deviations, as highlighted in the magnified views of the top and bottom rows. The high accuracy of our localisation along the trajectory is shown in Figure 4 (top) for *Forest II*, which is also noted by the precise registration of air-ground submaps displayed on the bottom snapshot.

Figure 5 presents the statistical analysis of all evaluated methods using absolute translation and heading errors as metrics compared against the ground truth. Since the baselines *MCLoc3D* and *Wheel Odom* can only provide poses in $SE(2)$, we used the 2D pose coordinates (x and y) and heading angle θ in the error calculation of all methods for a fair comparison. As seen, our method *FGLoc6D* outperformed all the baselines for both datasets in the estimation

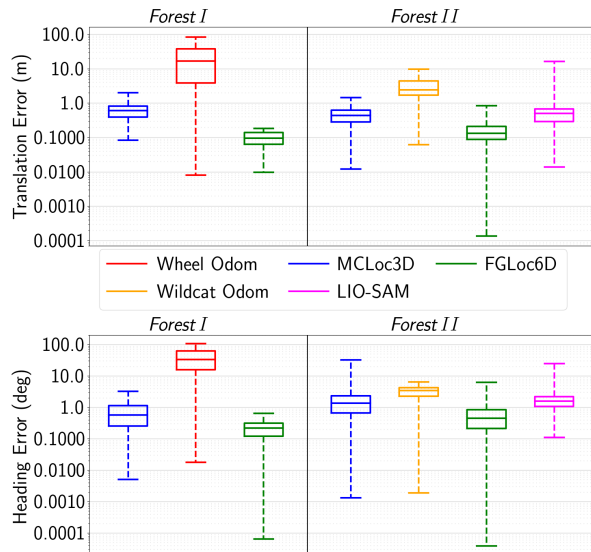


Fig. 5: Comparison of the absolute translation (top) and heading (bottom) errors of distinct pose estimation methods with respect to the ground truth. Dataset *Forest I*: our localisation errors compared to Wheel Odometry and *MCLoc3D* solutions. Dataset *Forest II*: our localisation errors compared with Wildcat Odometry, LIO-SAM and *MCLoc3D*. Our presented method notably outperforms all baselines.

of both position (top) and orientation (bottom), showing a significant improvement over our previous localisation *MCLoc3D*. Drift strongly affects *Wheel Odom* due to wheel slippage over the terrain, having the worse performance ($\sim 20\text{ m}$ position errors). Although the lidar-inertial odometry counterparts, *i.e.*, *Wildcat Odom* and LIO-SAM, demonstrate lower position and heading errors in *Forest II* compared to *Wheel Odom*, their maximum position errors are larger than 10 meters, revealing the impact of error accumulation. Furthermore, errors of odometry-based methods can grow unbounded in open-loop trajectories, preventing their use in robotic downstream tasks. In contrast, *FGLoc6D*'s incorporation of graph optimisation with aerial map and lidar odometry factors results in drift-free, accurate pose estimates, with most errors below 0.25 m in both datasets *Forest I* and *II* (see Figure 5 (a) and (b)).

We also evaluated the full 6DoF pose errors of our *FGLoc6D* method and compared it against a factor-graph optimisation framework integrating GPS data as reference factors with Wildcat Odometry. As seen in Table I, our translation error (Trans. Error) and orientation error (Rot. Error) remain accurate, with RMSE of 0.23 m and 1.16° , respectively. In contrast, the GPS solution showed signifi-

		RMSE	median	mean	std.dev	max
<i>FGLoc6D</i>	Trans. Error (m)	0.23	0.14	0.18	0.15	0.83
	Rot. Error (deg)	1.16	0.65	0.88	0.76	6.32
GPS + Odom	Trans. Error (m)	2.96	2.44	2.65	1.32	8.15
	Rot. Error (deg)	5.44	3.96	4.78	2.59	11.75

TABLE I: Evaluation of 6DoF pose errors in *Forest II* comparing *FGLoc6D* with a GPS-based factor graph localisation baseline. Trans. Error indicates absolute translation (3DoF) errors, and Rot. Error shows absolute rotation (3DoF) errors, both relative to the ground truth trajectory.

Runtime(s)	Odometry	Registration	FG Optimisation	Re-Localisation
mean	0.055	0.288	0.038	0.418
std.dev	± 0.012	± 0.063	± 0.024	± 0.189

TABLE II: Runtime analysis of each component in our global localisation framework.

cantly higher RMSE, 2.96 m and 5.44° and a large maximum position error (8.15 m). This experiment highlights that degraded GPS measurements are unsuitable for accurate position estimation beneath the canopy, even when fused with lidar-inertial odometry. Additionally, these findings underscore the robustness and accuracy of our proposed localisation approach in complex forest environments.

D. Runtime Analysis

To demonstrate that our presented system can run online, we evaluated the computation time for each component. The timing results are collected by running the pre-trained deep learning models on GPU, and the rest of the pipeline on CPU as described in Section IV. Table II reports a breakdown of individual modules' runtime in our pipeline. The total runtime (for the *Forest II* experiment) is less than a second, allowing the system to run online. Once re-localisation is performed, the low-level odometry and back-end optimisation altogether can run at $\sim 3\text{ Hz}$.

V. CONCLUSION AND FUTURE WORK

We introduced a 6DoF pose estimation framework that integrates cross-view factor graph optimisation with a lightweight CNN-based deep-learned re-localisation technique, enabling precise global localisation of a ground (below canopy) robot against an aerial (above canopy) map in forest environments. Extensive experiments in challenging forest conditions demonstrate our method's superior accuracy and robustness compared to existing baselines. A key technical achievement is the formulation of the localisation problem as a bipartite graph, combining ground-to-aerial unary factors with model-based and data-driven models for global optimisation. Additionally, the use of GICP enhances point cloud registration by reducing distributional differences between ground and aerial submaps, thus improving the precision of robot pose estimates. The real-time capability of the system has been validated through runtime analysis, illustrating that the presented pipeline can operate efficiently under practical conditions. In future work we will explore transformer-based re-localisation approaches for greater generalisability across varying forest environments and the use of GPU acceleration for faster registration and more scalable computation.

ACKNOWLEDGMENTS

The authors thank CSIRO Robotics members for their hardware and software support. This work was partially supported by the SILVANUS Project through European Commission Funding on the Horizon 2020 under Grant H2020-LC-GD-2020 and Grant 101037247.

REFERENCES

- [1] M. Aftatah, A. Lahrech, and A. Abounada, "Fusion of GPS/INS/Odometer measurements for land vehicle navigation with GPS outage," in *2016 2nd Int. Conf. on Cloud Computing Technologies and Applications*. IEEE, 2016, pp. 48–55.
- [2] P. Srinivas and A. Kumar, "Overview of Architecture for GPS-INS Integration," in *2017 Recent Developments in Control, Automation Power Engineering (RDCAPE)*, 2017, pp. 433–438.
- [3] T. Shan and B. Englot, "LeGO-LOAM: Lightweight and Ground-Optimized Lidar Odometry and Mapping on Variable Terrain," in *2018 IEEE/RSJ Int. Conf. on Intelligent Robots and Systems (IROS)*, 2018, pp. 4758–4765.
- [4] D. Dusha and L. Mejias, "Error analysis and attitude observability of a monocular GPS/visual odometry integrated navigation filter," *The Int. Journal of Robotics Research*, vol. 31, no. 6, pp. 714–737, 2012.
- [5] A. S. Aguiar, F. N. D. Santos, J. B. Cunha, H. Sobreira, and A. J. Sousa, "Localization and Mapping for Robots in Agriculture and Forestry: A Survey," *Robotics*, vol. 9, no. 4, pp. 1–23, 2020.
- [6] M. Miettinen, M. Öhman, A. Visala, and P. Forsman, "Simultaneous Localization and Mapping for Forest Harvesters," *IEEE Int. Conf. on Robotics and Automation*, no. April, pp. 517–522, 2007.
- [7] S. W. Chen, G. V. Nardari, E. S. Lee, C. Qu, X. Liu, R. A. F. Romero, and V. Kumar, "SLOAM: Semantic Lidar Odometry and Mapping for Forest Inventory," *IEEE Robotics and Automation Letters*, vol. 5, no. 2, pp. 612–619, 2020.
- [8] F. Nie, W. Zhang, Y. Wang, Y. Shi, and Q. Huang, "A Forest 3-D Lidar SLAM System for Rubber-Tapping Robot Based on Trunk Center Atlas," *IEEE/ASME Transactions on Mechatronics*, pp. 1–11, 2021.
- [9] T. Shan, B. Englot, D. Meyers, W. Wang, C. Ratti, and D. Rus, "LIO-SAM: Tightly-coupled Lidar Inertial Odometry via Smoothing and Mapping," in *2020 IEEE/RSJ Int. Conf. on Intelligent Robots and Systems (IROS)*. IEEE, 2020, pp. 5135–5142.
- [10] A. Kukko, R. Kajaluoto, H. Kaartinen, V. V. Lehtola, A. Jaakkola, and J. Hyypä, "Graph SLAM correction for single scanner MLS forest data under boreal forest canopy," *ISPRS Journal of Photogrammetry and Remote Sensing*, vol. 132, pp. 199–209, 2017.
- [11] L. C. de Lima, M. Ramezani, P. Borges, and M. Brüning, "Air-Ground Collaborative Localisation in Forests Using Lidar Canopy Maps," *IEEE Robotics and Automation Letters*, vol. 8, no. 3, pp. 1818–1825, 2023.
- [12] J. Kim and J. Kim, "Fusing Lidar Data and Aerial Imagery with Perspective Correction for Precise Localization in Urban Canyons," *IEEE Int. Conf. on Intelligent Robots and Systems*, pp. 5298–5303, 2019.
- [13] T. Tang, D. De Martini, and P. Newman, "Get to the Point: Learning Lidar Place Recognition and Metric Localisation Using Overhead Imagery," *Robotics: Science and Systems XVII*, 2021.
- [14] S. Wang, C. Nguyen, J. Liu, Y. Zhang, S. Muthu, F. A. Maken, K. Zhang, and H. Li, "View From Above: Orthogonal-View aware Cross-view Localization," in *Proceedings of the IEEE/CVF Conference on Computer Vision and Pattern Recognition (CVPR)*, June 2024, pp. 14 843–14 852.
- [15] F. Fervers, S. Bullinger, C. Bodensteiner, M. Arens, and R. Stiefelhagen, "Uncertainty-aware Vision-based Metric Cross-view Geolocalization," in *Proceedings of the IEEE/CVF Conference on Computer Vision and Pattern Recognition*, 2023, pp. 21 621–21 631.
- [16] C. Subakan, M. Ravanelli, S. Cornell, M. Bronzi, and J. Zhong, "Attention is all you need in speech separation," in *ICASSP 2021-2021 IEEE Int. Conf. on Acoustics, Speech and Signal Processing (ICASSP)*. IEEE, 2021, pp. 21–25.
- [17] N. Vandapel, R. R. Donamukkala, and M. Hebert, "Unmanned Ground Vehicle Navigation Using Aerial Lidar Data," *Int. Journal of Robotics Research*, vol. 25, no. 1, pp. 31–51, 2006.
- [18] A. E. Johnson, "Spin-Images: A Representation for 3-D Surface Matching," Ph.D. dissertation, Carnegie Mellon University, August 1997.
- [19] A. Viswanathan, B. R. Pires, and D. Huber, "Vision Based Robot Localization by Ground to Satellite Matching in GPS-denied Situations," *IEEE Int. Conf. on Intelligent Robots and Systems*, pp. 192–198, 2014.
- [20] O. Shalev and A. Degani, "Canopy-Based Monte Carlo Localization in Orchards Using Top-View Imagery," *IEEE Robotics and Automation Letters*, vol. 5, no. 2, pp. 2403–2410, 2020.
- [21] M. Hussein, M. Renner, M. Watanabe, and K. Iagnemma, "Matching of Ground-Based LiDAR and Aerial Image Data for Mobile Robot Localization in Densely Forested Environments," *IEEE Int. Conf. on Intelligent Robots and Systems*, pp. 1432–1437, 2013.
- [22] P. J. Besl and N. D. McKay, "A Method for Registration of 3-D Shapes," in *Sensor fusion IV: control paradigms and data structures*, vol. 1611. Spie, 1992, pp. 586–606.
- [23] K. Koide, S. Oishi, M. Yokozuka, and A. Banno, "Tightly Coupled Range Inertial Localization on a 3D Prior Map Based on Sliding Window Factor Graph Optimization," in *2024 IEEE Int. Conf. on Robotics and Automation (ICRA)*, 2024, pp. 1745–1751.
- [24] G. Kim and A. Kim, "Scan Context: Egocentric Spatial Descriptor for Place Recognition within 3D Point Cloud Map," in *2018 IEEE/RSJ Int. Conf. on Intelligent Robots and Systems (IROS)*. IEEE, 2018, pp. 4802–4809.
- [25] S. Salti, F. Tombari, and L. Di Stefano, "SHOT: Unique signatures of histograms for surface and texture description," *Computer Vision and Image Understanding*, vol. 125, pp. 251–264, 2014.
- [26] R. Dubé, D. Dugas, E. Stumm, J. Nieto, R. Siegwart, and C. Cadena, "SegMatch: Segment Based Place Recognition in 3D Point Clouds," in *2017 IEEE Int. Conf. on Robotics and Automation (ICRA)*. IEEE, 2017, pp. 5266–5272.
- [27] R. Dubé, A. Cramariuc, D. Dugas, J. Nieto, R. Siegwart, and C. Cadena, "SegMap: 3D Segment Mapping using Data-Driven Descriptors," *Robotics: Science and Systems Online Proceedings*, vol. 14, 2018.
- [28] G. Tinchev, A. Penate-Sanchez, and M. Fallon, "Learning to See the Wood for the Trees: Deep Laser Localization in Urban and Natural Environments on a CPU," *IEEE Robotics and Automation Letters*, vol. 4, no. 2, pp. 1327–1334, 2019.
- [29] F. Radenović, G. Toliás, and O. Chum, "Fine-Tuning CNN Image Retrieval with No Human Annotation," *IEEE Transactions on Pattern Analysis and Machine Intelligence*, vol. 41, no. 7, pp. 1655–1668, 2018.
- [30] R. Arandjelovic, P. Gronat, A. Torii, T. Pajdla, and J. Sivic, "NetVLAD: CNN architecture for weakly supervised place recognition," in *Proceedings of the IEEE Conference on Computer Vision and Pattern Recognition (CVPR)*, 2016, pp. 5297–5307.
- [31] J. Komorowski, M. Wysoczanska, and T. Trzcinski, "EgoNN: Egocentric Neural Network for Point Cloud Based 6DoF Relocalization at the City Scale," *IEEE Robotics and Automation Letters*, vol. 7, no. 2, pp. 722–729, 2021.
- [32] D. Cattaneo, M. Vaghi, and A. Valada, "LCDNet: Deep Loop Closure Detection and Point Cloud Registration for LiDAR SLAM," *IEEE Transactions on Robotics*, vol. 38, no. 4, pp. 2074–2093, 2022.
- [33] K. Vidanapathirana, P. Moghadam, S. Sridharan, and C. Fookes, "Spectral Geometric Verification: Re-Ranking Point Cloud Retrieval for Metric Localization," *IEEE Robotics and Automation Letters*, vol. 8, no. 5, pp. 2494–2501, 2023.
- [34] M. Ramezani, E. Griffiths, M. Haghghat, A. Pitt, and P. Moghadam, "Deep Robust Multi-Robot Re-Localisation in Natural Environments," in *2023 IEEE/RSJ Int. Conf. on Intelligent Robots and Systems (IROS)*. IEEE, 2023, pp. 3322–3328.
- [35] P. C. Lusk, K. Fathian, and J. P. How, "CLIPPER: A Graph-Theoretic Framework for Robust Data Association," in *2021 IEEE Int. Conf. on Robotics and Automation (ICRA)*. IEEE, 2021, pp. 13 828–13 834.
- [36] J. Li and G. H. Lee, "USIP: Unsupervised Stable Interest Point Detection from 3D Point Clouds," in *Proceedings of the IEEE/CVF Int. Conf. on computer vision*, 2019, pp. 361–370.
- [37] M. Ramezani, K. Khosoussi, G. Catt, P. Moghadam, J. Williams, P. Borges, F. Pauling, and N. Kottege, "Wildcat: Online Continuous-Time 3D Lidar-Inertial SLAM," *arXiv preprint arXiv:2205.12595*, 2022.
- [38] A. Segal, D. Haehnel, and S. Thrun, "Generalized-ICP," in *Robotics: science and systems*, vol. 2, no. 4. Seattle, WA, 2009, p. 435.
- [39] F. Dellaert and G. Contributors, "borglab/gtsam," May 2022. [Online]. Available: <https://github.com/borglab/gtsam>
- [40] K. Koide, M. Yokozuka, S. Oishi, and A. Banno, "Voxelized GICP for Fast and Accurate 3D Point Cloud Registration," in *2021 IEEE Int. Conf. on Robotics and Automation (ICRA)*, 2021, pp. 11 054–11 059.
- [41] D. P. Kingma and J. Ba, "Adam: A Method for Stochastic Optimization," *CoRR*, Dec. 2014.
- [42] W. Zhang, J. Qi, P. Wan, H. Wang, D. Xie, X. Wang, and G. Yan, "An Easy-to-Use Airborne LiDAR Data Filtering Method Based on Cloth Simulation," *Remote Sensing*, vol. 8, no. 6, p. 501, June 2016.